Acta Crystallographica Section D
**Biological Crystallography**
ISSN 0907-4449

# In-plate protein crystallization, *in situ* ligand soaking and X-ray diffraction

**Albane le Maire,[a,b] Muriel Gelin,[a,b] Sylvie Pochet,[c] François Hoh,[a,b] Michel Pirocchi,[d,e,f] Jean-François Guichou,[a,b] Jean-Luc Ferrer[d,e,f]* and Gilles Labesse[a,b]***

[a]CNRS, UMR5048 – Université Montpellier 1 et 2, Centre de Biochimie Structurale, F-34090 Montpellier, France, [b]INSERM, U1054, F-34090 Montpellier, France, [c]Unité de Chimie et Biocatalyse, Institut Pasteur, F-75015 Paris, France; CNRS, URA2128, F-75015 Paris, France, [d]CEA, Institut de Biologie Structurale/Groupe Synchrotron, F-38027 Grenoble, France, [e]CNRS, Institut de Biologie Structurale/Groupe Synchrotron, F-38027 Grenoble, France, and [f]Université Joseph Fourier – Grenoble 1, Institut de Biologie Structurale/Groupe Synchrotron, F-38027 Grenoble, France.

Correspondence e-mail: jean-luc.ferrer@ibs.fr, labesse@cbs.cnrs.fr



Received 18 April 2011
Accepted 14 June 2011

**PDB References:** Erk-2–6PB, 3qyw; Erk-2–Z8B, 3qyz; CypD, 3qyu.

X-ray crystallography is now a recognized technique for ligand screening, especially for fragment-based drug design. However, protein crystal handling is still tedious and limits further automation. An alternative method for the solution of crystal structures of proteins in complex with small ligands is proposed. Crystallization drops are directly exposed to an X-ray beam after cocrystallization or soaking with the desired ligands. The use of dedicated plates in connection with an optimal parametrization of the G-rob robot allows efficient data collection. Three proteins currently under study in our laboratory for ligand screening by X-ray crystallography were used as validation test cases. The protein crystals belonged to different space groups, including a challenging monoclinic case. The resulting diffraction data can lead to clear ligand recognition, including indication of alternating conformations. These results demonstrate a possible method for automation of ligand screening by X-ray crystallography.

## 1. Introduction

X-ray crystallography is now the most classical method of obtaining structural information on biological macromolecules. By mid-2010, 46 872 biological macromolecule structures had been deposited in the Protein Data Bank (PDB; www.rcsb.org/pdb; Rose *et al.*, 2011), with most of them being obtained by X-ray crystallography. The importance of X-ray crystallography in the field of rational drug design is now well established. It includes determination of the mode of binding of known ligands for hit-to-lead optimization and also the identification of weak ligands through fragment screening (Murray & Blundell, 2010; Schulz & Hubbard, 2009; Chessari & Woodhead, 2009).

Although widely used, this technique includes several difficult steps. It requires the production of significant amounts of pure and stable material (protein, nucleic acid *etc.*), crystallization, harvesting, cryocooling, data collection on laboratory or synchrotron X-ray sources and data processing to build a model of the structure.

Significant improvements have been made to X-ray sources and data processing is now highly automated (Joachimiak, 2009; Cymborowski *et al.*, 2010). Automated crystallization assays are performed using dedicated robots and pre-established conditions. Nanodispensers have significantly improved the throughput of crystallogenesis by decreasing the amount of material required.

However, the detection and handling of crystals to be used for data collection remains an important bottleneck. A previous breakthrough in the selection of good-quality crystals has been described. As an alternative to visualization of crystallization drops, the scanning of crystallization plates with

an X-ray beam has been developed (Jacquamet *et al.*, 2004). Its advantages are threefold: (i) it provides direct access to relevant information (diffraction, crystal quality and nature and, in many cases, unit-cell parameters, space group *etc.*), (ii) the method can be fully automated with a high reliability compared with the shape-recognition software used in the classical automated visualization setup and (iii) this analysis can be carried out without any manipulation of individual crystals, thus preserving the crystal integrity, in contrast to the classical procedure which includes physical manipulation of individual crystals, soaking in cryoprotectants and cryocooling, which are all steps that could potentially damage the crystal. Nevertheless, these crystallization plates and their handling limited the possibility of collecting sufficient diffraction data, preventing routine use in structure determination.

In parallel, the rapid development of ligand screening by X-ray crystallography has led to an urgent need for efficient and possibly fully automated methods for cocrystallization or soaking and subsequent structure determination with little crystal handling.

Firstly, new plates with improved geometry and polymers were designed. Meanwhile, the G-Rob robot (developed on beamline FIP-BM30A at the ESRF and commercialized by NatX-ray, Grenoble, France) was adapted to collect diffraction data at various tilting angles (initially −25° to +25° and then −40° to +40°). A similar development at SLS beamline X06DA now enables *in situ* X-ray diffraction screening to allow the rapid selection of crystals suitable for structure determination (Bingel-Erlenmeyer *et al.*, 2011). Our aim was first to check the possible detection of a ligand bound to a protein. The examples described here demonstrate different cases of cocrystallization or soaking with a ligand as well as the use of low- and high-symmetry protein crystals. The quality of the data was sufficient to analyze in detail the mode of binding, the geometry of the active site and local structural rearrangements.

These results indicate that this methodology can be widely used for ligand screening by X-ray crystallography.

## 2. Materials and methods

### 2.1. A new low-profile plate

A new plate was designed to limit absorption by the matter surrounding the crystal drop (CrystalQuick X from Greiner Bio-One, Germany), as shown in Fig. 1. This was achieved by reducing the thickness of the well bottom to 300 µm and by the choice of an adapted material: the Cyclic Olefin Copolymer, a polyolefin with low birefringence properties. This resulted in a significantly reduced scattering profile (Bingel-Erlenmeyer *et al.*, 2011). Similarly, the profile of the reservoir and the drop location were optimized to permit the use of a large angle range, making it possible to collect up to an 80° total range at 3.45 Å resolution on a synchrotron beamline at 0.9 Å wavelength, 2.7 Å resolution using a molybdenum source or 5.9 Å resolution using a copper source, allowing the collection of a complete data set in many cases.

Initial attempts were made with the lower and upper limits set to −25° and +25°, respectively. This implied the collection of three incomplete data sets in the case of the monoclinic crystals of Erk-2 (see below) to obtain an 83% complete data set. Further improvements in the available angles (−40° to


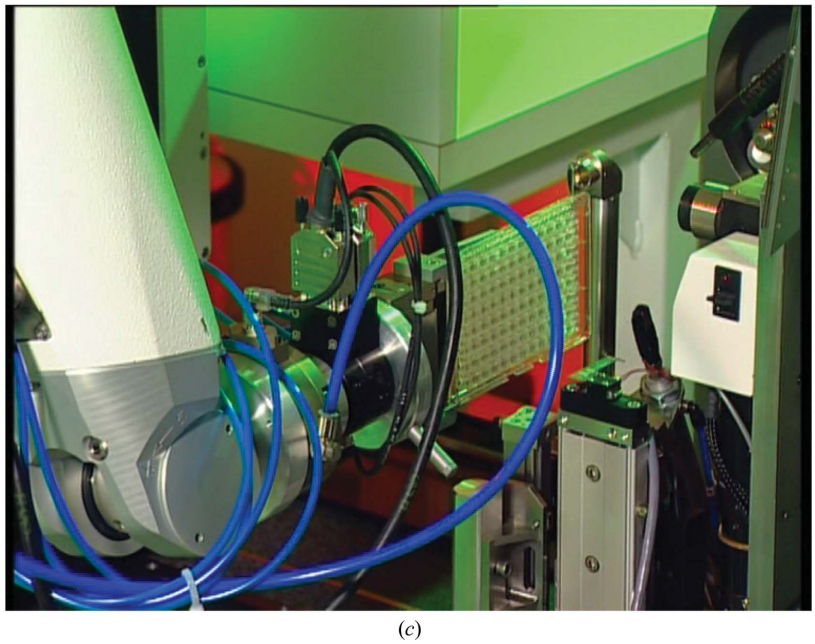


**Figure 1**
(*a*) View of the new 96-well CrystalQuick X plates (Greiner Bio-One) used for crystallogenesis and *in situ* diffraction. (*b*) Detailed view of the geometry of the plate well. (*c*) View of the plate hold by the CATS/G-Rob system in the X-ray beam during data collection.

+40°) for plate inclination led to almost complete data sets using only one crystal even in the case of the monoclinic space group. In all the test cases the crystals did not suffer significantly from their exposure to the X-ray beam.

### 2.2. In-plate cocrystallization or soaking

Crystallization drops were prepared with a Cartesian HoneyBee X8 crystallization robot (Genomic Solutions Inc.) equipped with eight independent needles and a liquid-detection system. For crystallization, 96-well CrystalQuick X plates (Greiner Bio-One) with square drop locations were used. The wells were filled with 70 µl crystallization buffer, and 250 nl of the reservoir was mixed with 250 nl of the protein sample prior to deposition on the drop location. The large volume of the protein drop allowed the subsequent addition of a ligand solubilized in 100% DMSO (50 nl) while maintaining the final concentration in solvent as low as possible (10% in our test cases). The plate was then sealed with a transparent plastic film (Greiner G-676070) and kept at 291 K until beam time became available.

### 2.3. Protein samples

For the tests, we used well behaved proteins that had previously been studied in our laboratory. They crystallized readily and diffracted well. Furthermore, we took advantage of their different space groups (monoclinic, orthorhombic and tetragonal) to evaluate the limit of the currently available range of orientation angles for the plates.

The crystallization of the protein kinase Erk-2 from rat has been described previously (Zhang *et al.*, 1994) and was only slightly modified. The precipitant solution now contained 2 m*M* $MgSO_4$ in addition to the previously used precipitant. The reproducibility of crystal growth was further improved by using microseeding beeds (Hampton Research, USA). Up to 15 high-quality crystals could be grown in a 96-well plate within a few days. Within two weeks, data were collected using the G-rob plate handler and the X-ray beam at beamline FIP-BM30A (ESRF). The first attempts were made with an adenine derivative, 2-amino-6-(3-bromophenyl)purine. This chemical compound corresponds to a fragment and was synthesized following a classical chemical route (data not shown). The second compound used was an adenosine derivative bearing a Br atom at its C8 position and a derivatization at its 5′ position. In both cases, the crystal shapes and lattice were little affected by ligand addition.

The crystallization of the complex between human RXR$\alpha$ ligand-binding domain and an organotin (tributyltin; TBT) in the presence of a co-activator peptide (Tif2) has previously been reported (le Maire *et al.*, 2009). Crystallization of this ternary complex was reproduced in the new plate and large crystals appeared within a few days.

The crystallization of a variant of human cyclophilin CypD bearing a K133I mutation has previously been described (Schlatter *et al.*, 2005) and could be reproduced in the new plate with little modification. The reproducibility of crystal growth was further improved using microseeding beeds (Hampton Research, USA). However, this remained a limiting factor, with only a handful of high-quality crystals being grown within a few days.

### 2.4. Data collection

Data were collected on the FIP-BM30A beamline at the ESRF (Grenoble, France) equipped with an ADSC Q315r CCD detector. Centring was manually performed for each crystal using solely the focus at zero tilting as a quality estimate. The diffraction quality was then tested at various angles. Residual off-centring, after taking into account refraction across the plastic, was corrected in a trial-and-error manner.

### 2.5. Data processing

Data processing was performed using *MOSFLM* (Leslie, 2006) and *SCALA* from the *CCP*4 suite (Winn *et al.*, 2011). Molecular replacement was performed using *MOLREP* (Vagin & Teplyakov, 2010). Structure refinement was performed in parallel using *REFMAC*5 (Murshudov *et al.*, 2011) or *PHENIX* (Adams *et al.*, 2010). In the case of the high-resolution structure of CypD, manual model building was performed using *Coot* (Emsley & Cowtan, 2004).

## 3. Results

### 3.1. Crystal structure of Erk-2 in complex with 6PB

As a first test, we soaked a crystal of protein kinase Erk-2 with a brominated arylpurine derivative. This compound, referred to in the following as 6PB, corresponds to a privileged pharmacophore for protein kinases bearing a brominated phenyl group. This compound was known to bind from a previous experiment using cryocooled crystals (see below).

The crystals of Erk-2 diffracted well, but their low symmetry represented a challenge for the collection of a complete data set owing to the geometric limit in plate handling.

X-ray data were collected from four distinct crystals from four different crystallization drops. The best three data sets were merged to obtain an 83% complete data set at 2.14 Å resolution. The structure was solved straightforwardly using isomorphous replacement. The electron density assigned to the ligand was clearly visible at all steps although the ligand had been omitted (data not shown). In parallel, to limit any potential bias, multiple molecular replacements were performed using *MOLREP* (Vagin & Teplyakov, 2010) and all available structures of Erk-2 (and some potentially closely related protein kinases) using the *@TOME*-2 server (Pons & Labesse, 2009). The results are available at http://atome.cbs.cnrs.fr/AT2/EG/47415/atome.html. The best solution appeared to be that obtained using PDB entry 1gol (Robinson *et al.*, 1996) according to the *R* factor 30.2%), although the contrast appeared to be better (21.1 *versus* 16.6) for the third best solution (PDB entry 4erk, with an *R* factor of 34.7%; Wang *et al.*, 1998). After ten steps of rigid-body refinement using *REFMAC*5 (Murshudov *et al.*, 1997), the *R* factor was as low as 27.2% ($R_{\rm free}$ = 27.6%). The electron density already revealed some variations in side-chain

**Table 1**
Data-collection and refinement statistics for all complexes described in this study.

Values in parentheses are for the outermost resolution shell.

| Protein ligand | Erk-2–6PB | Erk-2–6PB | Erk-2–Z8B | Erk-2–Z8B | RXR–TBT | Native CypD |
|---|---|---|---|---|---|---|
| Data collection | Plate | Cryoloop | Plate | Cryoloop | Plate | Plate |
| Beamline | BM30 | ID14-2 | BM30 | ID14-2 | BM30 | BM30 |
| Angular range (°) | 50 + 44 + 50 | | 80 | | 50 | 60 + 17 |
| No. of crystals | 3 | 1 | 1 | 1 | 1 | 2 |
| Space group | $P2_1$ | $P2_1$ | $P2_1$ | $P2_1$ | $P4_32_12$ | $P4_12_12$ |
| Unit-cell parameters | | | | | | |
| $a$ (Å) | 49.1 | 49.0 | 49.2 | 48.7 | 66.3 | 57.9 |
| $b$ (Å) | 71.3 | 70.2 | 71.1 | 70.2 | 66.3 | 57.9 |
| $c$ (Å) | 60.8 | 60.1 | 60.9 | 59.5 | 112.2 | 88.5 |
| $\beta$ (°) | 109.2 | 108.7 | 109.3 | 108.5 | | |
| No. of molecules in asymmetric unit | 1 | 1 | 1 | 1 | 1 | 1 |
| Wavelength (Å) | 0.97974 | 0.93300 | 0.97974 | 0.93300 | 0.97974 | 0.97974 |
| Resolution (Å) | 2.14 | 1.50 | 1.93 | 1.46 | 2.17 | 1.54 |
| $R_{\rm merge}$† (%) | 4.7 (10.5) | 3.8 (17.5) | 8.9 (45.2) | 3.0 (40.7) | 8.9 (46.5) | 6.1 (29.9) |
| $\langle I/\sigma(I)\rangle$ | 5.2 (5.7) | 11.5 (3.3) | 3.7 (1.3) | 11.4 (1.0) | 6.0 (2.1) | 25.7 (4.1) |
| Completeness (%) | 83.1 (80.5) | 91.7 (84.2) | 70.9 (74.3) | 95.1 (73.6) | 89.3 (97.6) | 86.2 (82.1) |
| Multiplicity | 2.7 (2.8) | 1.9 (1.4) | 1.8 (1.7) | 3.6 (1.9) | 2.8 (3.0) | 3.6 (2.5) |
| Wilson $B$ factor (Å$^2$) | 27.6 | 15.1 | 31.0 | 18.1 | 28.3 | 17.1 |
| Refinement | | | | | | |
| Resolution (Å) | 38.90–2.14 | 36.90–1.50 | 28.70–1.93 | 46.18–1.46 | 57.07–2.17 | 28.98–1.54 |
| No. of reflections | 18304 | 56567 | 20223 | 62682 | 11386 | 18518 |
| $R_{\rm work}$‡/$R_{\rm free}$§ (%) | 23.1/27.1 | 13.4/18.4 | 21.6/27.5 | 16.1/19.5 | 23.3/28.3 | 15.1/19.3 |
| No. of atoms | | | | | | |
| Protein | 2890 | 2862 | 2814 | 2942 | 1775 | 1282 |
| Ligand | 17 | 17 | 24 | 22 | 30 | — |
| Water | 0 | 468 | 224 | 458 | 83 | 126 |
| $B$ factors (Å$^2$) | | | | | | |
| Protein¶ | 15.8 | 16.5 | 26.8 | 24.6 | 30.2 | 17.1 |
| Ligand | 26.3 | 18.5 | 42.4 | 30.5 | 22.3 | — |
| Water | — | 35.4 | 32.4 | 38.2 | 34.7 | 32.4 |
| R.m.s. deviations†† | | | | | | |
| Bond lengths (Å) | 0.009 | 0.009 | 0.008 | 0.008 | 0.009 | 0.009 |
| Bond angles (°) | 1.19 | 1.10 | 1.14 | 1.09 | 1.16 | 1.21 |

† $R_{\rm merge} = \sum_{hkl}\sum_i |I_i(hkl) - \langle I(hkl)\rangle|/\sum_{hkl}\sum_i I_i(hkl) \times 100$. ‡ $R_{\rm work} = \sum_{hkl} ||F_{\rm obs}| - |F_{\rm calc}||/\sum_{hkl}|F_{\rm obs}| \times 100$. § $R_{\rm free}$ is calculated in the same way as $R_{\rm work}$ on a subset of reflections that were not used in the refinement (5%). ¶ $B$ factors for proteins do not include the anisotropic part simulated by the TLS parameters. †† Deviation from ideal values.

orientations as well as more pronounced but local rearrangements in some loops. In addition, extra electron density was clearly visible in the ATP-binding site. Ten steps of restrained refinement using *REFMAC*5 confirmed the first conclusion and lowered the $R$ factor to 24.7 ($R_{\rm free}$ = 28.2%). Ten steps of TLS refinement (Winn *et al.*, 2001) followed by final minimization (ten steps of restrained refinement) in *REFMAC*5 led to very clear electron density despite the lack of a manual rebuilding step ($R$ factor and $R_{\rm free}$ of 23.6% and 28.1%, respectively). The 2-aminopurine bearing a bromobenzyl group was clearly recognized (Fig. 2*b*). It appears in the same position as that observed in an equivalent but cryocooled sample obtained classically (Fig. 2*c*). The ligand was added using the 'FindLigand' function in *Coot* and a new round of restrained refinement was performed using *REFMAC*5. The final parameters of this partial refinement are given in Table 1 together with those for the classical refinement performed on the cryocooled crystal.

Alternatively, a fully automatic refinement was performed using the *PHENIX* suite (Adams *et al.*, 2010). We started from the same molecular refinement solution (PDB entry 1gol) as above. Firstly, a rigid-body refinement with $B$ factors and TLS was performed using default parameters (final $R_{\rm work}$ and $R_{\rm free}$ of 24.9% and 27.2%, respectively). Subsequently, a positional refinement (with $B$ factors and TLS) was performed (final $R_{\rm work}$ and $R_{\rm free}$ of 21.3% and 27.3%, respectively). In all cases, clear density was apparent in the ATP-binding site. *LigandFit* (Terwilliger *et al.*, 2007) was able to correctly place the 2-amino-6-(3-bromophenyl)purine (score of 70.1 and map CC of 0.79). The structures refined using the *PHENIX* and *CCP*4 suites showed an r.m.s.d. of 0.21 Å on 357 $C^\alpha$ atoms. In both cases the orientation of the ligand perfectly matches that computed using data at higher resolution (1.5 Å) and recorded from a cryocooled crystal. Similarly, the structures partially refined using the data at room temperature showed an r.m.s.d. from the structure solved at 100 K of ∼0.67 Å (over 341 common $C^\alpha$ atoms). In all cases, the interactions observed between the ligand and the protein matched the privileged interactions in protein kinases. They included a network of hydrogen bonds between the 2-aminopurine edge (through N9, N3 and N2) and the backbone atoms of the so-called hinge (residues Leu105–Met106 in Erk-2). In parallel, the purine is sandwiched by two conserved and hydrophobic residues: Ala50 and Leu154. The same orientation is observed in CDK2 in complex with a distinct 2-aminopurine compound (Pratt *et al.*, 2006; PDB entry 2iw9). Additional contacts involved Val37 and the bromophenyl group, which also points towards Gly30 and Gly32 from the glycine-rich loop. Accordingly, this ligand corresponds to an interesting fragment from which one may derive better ligands.

The data obtained at room temperature in the crystallization plate compared favourably with the data collected from a cryocooled crystal. Indeed, the ligand could be readily recognized after only a few cycles of automatic refinement. However, in this case the low symmetry coupled with the limited inclination range of the plate were clearly a drawback as several crystals were required. Furthermore, the strategy could not be significantly improved with the current setup as the crystal orientation could not be changed to improve the data-set completeness efficiently. This prompted us to further improve the experiment by allowing larger plate inclinations of angles of −40°/+40° instead of −25°/+25°. This new

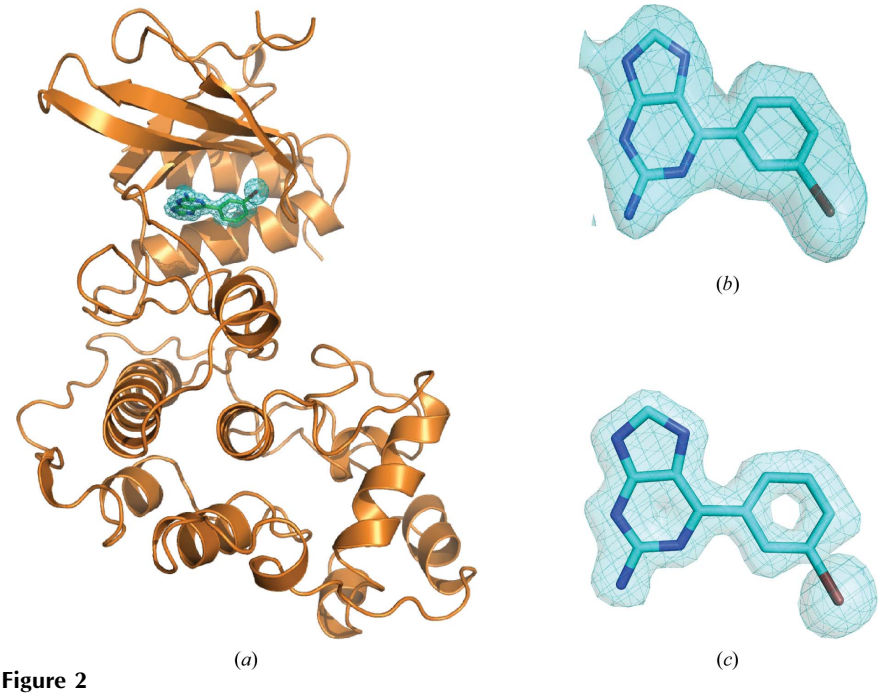


**Figure 2**
*In cristallo* screening. Crystal structures of an adenine derivative bound to the Erk-2 active site. (*a*) Global structure of Erk-2 bound to 6-bromophenylpurine solved at high resolution and at 100 K. The structure is shown as an orange ribbon and the ligand as sticks in CPK colours. (*b*) Enlargement of the active site and view of the extra electron density in the active site of Erk-2 observed after partial refinement using the data set collected at room temperature. The ligand is shown for clarity but was not included in the refinement (see text). (*c*) View of the ligand 6-bromophenylpurine and its electron density in the active site of Erk-2 after final refinement at high resolution using data recorded at 100 K. In all panels, the $2F_o - F_c$ electron-density map contoured at $0.9\sigma$ was computed with the ligand molecule omitted from the Fourier synthesis. The electron density is drawn as a mesh and a surface in cyan. This figure was generated using the program *PyMOL* (http://www.pymol.org).

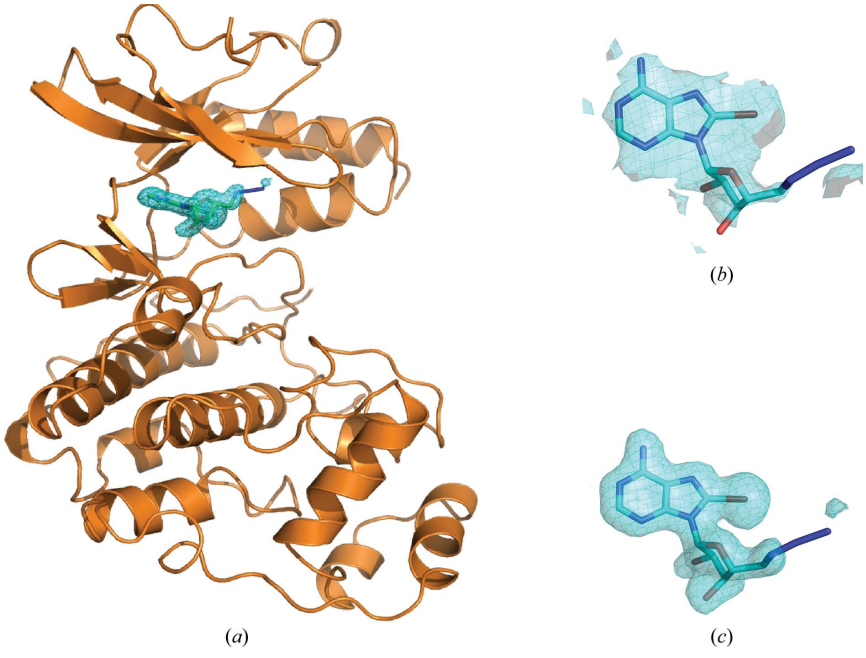


**Figure 3**
*In cristallo* screening. Crystal structures of an adenosine derivative bound to the Erk-2 active site. (*a*) Global structure of Erk-2 bound to 8-bromo-5′-amino-5′-deoxyadenosine (Z8B) solved at high resolution and at 100 K. Structure and density are drawn as in Fig. 2. (*b*) As in Fig. 2(*b*) but for the ligand Z8B. (*c*) As in Fig. 2(*c*) but for the ligand Z8B. In all panels, the $2F_o - F_c$ electron-density map contoured at $0.9\sigma$ was computed with the ligand molecule omitted from the Fourier synthesis. This figure was generated using the program *PyMOL* (http://www.pymol.org).

geometry was used for the following structure of Erk-2 in complex with another ligand.

### 3.2. Crystal structure of Erk-2 in complex with Z8B

As a second test, we used a brominated adenosine derivative: 8-bromo-5′-azido-5′-deoxyadenosine (hereafter referred to as Z8B). It harbours an azidoribose, which is a more flexible substituent compared with that in the above example. Again, this chemical compound was known to bind from a previous experiment using cryocooled crystals (Fig. 3*a*; see below).

The new experimental capabilities were tested in another plate with new freshly grown Erk-2 crystals subsequently soaked with Z8B. Five large crystals were available for data collection in the two lanes used in this soaking assay. Most of them showed poor diffraction (∼3 Å) and appeared to be polycrystalline. However, one crystal diffracted very well. Owing to the larger range (−40° to +40°) for diffraction measurements that was made available on the beamline and the new crystallization plate, a 71% complete data set was recorded. The crystal again belonged to the monoclinic space group $P2_1$ and was isomorphous to our previous Erk-2 crystals. In order to limit the number of refinement steps and to avoid too strong a bias, a parallel molecular replacement was performed using *MOLREP* (Vagin & Teplyakov, 2010) through the *@TOME*-2 server (Pons & Labesse, 2009). Most structures of Erk-2 previously deposited in the PDB (Rose *et al.*, 2011) were tested in this step (http://atome.cbs.cnrs.fr/AT2/EG/23295/atome.html). The structure giving the best solution (according to the final *R* and contrast values) was used in a ten-step rigid-body refinement in *REFMAC*5 (Murshudov *et al.*, 1997). Clear electron density was visible in the ATP-binding pocket and the adenine ring could be recognized, while the bromo group and the ribose appeared slightly less clearly. Five steps of restrained refinement were performed using all data to 1.93 Å resolution. The extra electron density in the ATP-

binding cavity indicated that the bromine group was present, while the azido group was either mobile or labile (see Fig. 3*b*).

As above, *PHENIX* (Adams *et al.*, 2010) was used for fully automatic refinement and the resulting structure highlighted similar features. Despite the low completeness, the data were sufficient to indicate ligand binding and its rough orientation in the ATP-binding site. However, automatic docking into the density failed as the adenosine was placed in the active site but in two incorrect orientations (data not shown). The correct orientation (Fig. 3*c*) can be determined manually and matched the usual mode of binding of an adenosine in the active site of a protein kinase (as shown by Mg-ATP in PDB entry 1gol). The precise and automatic determination of the ligand conformation may require additional measurements or a higher resolution. The precise structure of the complex was determined using data recorded at higher resolution from a cryocooled crystal (Table 1). Compared with the structure in the complex with 6PB (see above), this new structure shows some rearrangements in the active site, mainly in the glycine-rich loop. These changes are necessary to accommodate the 5′-derivatization and suggest a way to increase the ligand size in order to improve its affinity.

This example shows that rapid ligand screening in plates can be performed even in the case of a low-symmetry space group (here monoclinic $P2_1$ with only one twofold symmetry). Manual refinement could lead to a medium-quality structure of the complex, while automatic and partial refinement already allows the recognition of the presence of a bound adenosine. This could prompt one to record supplementary data using either additional crystals present in the plate or by soaking, mounting and cryocooling one crystal for complete data recording.

### 3.3. Crystal structure of RXR in complex with an organotin

Using the new plate, we reproduced the cocrystallization of the nuclear receptor RXR$\alpha$ in complex with an organotin (tributyltin; hereafter referred to as TBT) and a co-activator peptide (Tif2). These crystals allowed us to collect high-quality data. 50 images were collected from a single crystal and were used to solve the structure of the RXR$\alpha$–TBT–Tif2 complex. This crystal appeared to be isomorphous to that previously described (space group $P4_32_12$) and diffracted to beyond 2.0 Å resolution. Scaling of the data provided us with an 89.3% complete data set (97.6% completeness in the outer resolution shell) at a resolution of 2.17 Å.

A number of structures of the receptor RXR in its active form (in complex with an agonist ligand and a coactivator peptide) have been published and could be used to solve the new structure. In order to evaluate the potential bias in using a too closely related structure, two distinct structures were used as a starting point for the refinement. One template corresponded to the same RXR–TBT–Tif2 complex as that solved from a cryocooled crystal (PDB entry 3e94; le Maire *et al.*, 2009) and the second corresponded to a reference structure of the RXR–9-*cis*-RA–SRC1 complex (PDB entry 1k74; Xu *et al.*, 2001). In both cases the small chemical ligands were omitted during the initial refinement. Firstly, a ten-step rigid-body refinement using *REFMAC*5 (Murshudov *et al.*, 1997) was performed. The resulting $R$ factors were 34 and 40%, respectively. In both cases, clear density was visible in the $F_o - F_c$ map and was attributed to an Sn atom. This partial refinement was already sufficient to identify the ligand and its binding mode.

Alternatively, as in the case of Erk-2, a semi-automatic procedure was applied to limit any bias in the refinement. Molecular replacements using all available RXR structures were performed in parallel using *MOLREP* (Vagin &

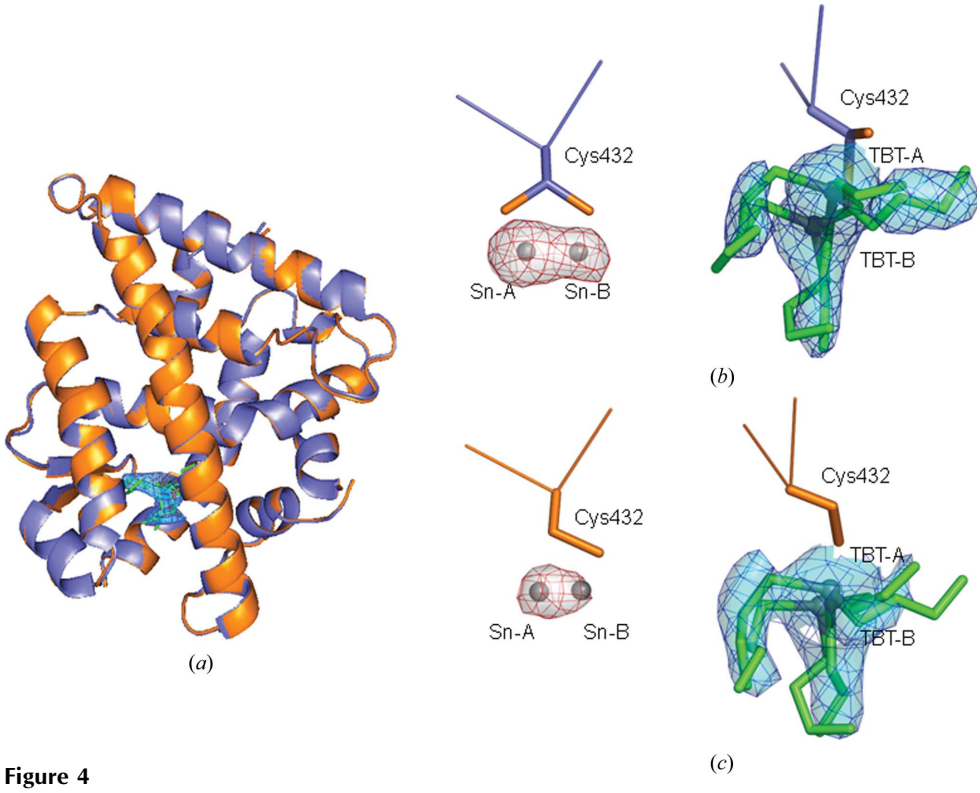


**Figure 4**
*In cristallo* screening. Crystal structures of RXR$\alpha$ complexed with an organotin (TBT). (*a*) Superposition of the structure solved from a cryocooled crystal (blue; PDB entry 3e94) with the structure solved from a crystal at room temperature (orange). (*b*) OMIT maps of the electron density in the active site of the structure from a cryocooled crystal (PDB entry 3e94). $F_o - F_c$ (red) and $2F_o - F_c$ (blue) maps are contoured at 9.0$\sigma$ and 1.0$\sigma$, respectively. (*c*) As Fig. 2(*b*) but for the structure refined from the data obtained at room temperature in the new plate (see text). This figure was generated using the program *PyMOL* (http://www.pymol.org).

Teplyakov, 2010) through the *@TOME*-2 server (Pons & Labesse, 2009). The results can be found at http://atome.cbs.cnrs.fr/AT2/EG/60575/atome.html. Two distinct structures were used as a starting point for the refinement. The first template corresponded to the same RXR–TBT–Tif2 complex as previously solved from a cryocooled crystal (PDB entry 3e94). As expected, the *R*-factor and contrast values for this model were the best (43.1% and 8.05, respectively). The second template corresponded to the structure of RXR in a binary complex with retinoic acid (PDB entry 1fby; Egea *et al.*, 2000) and its statistics of molecular replacement were poorer but acceptable (*R* factor of 50.3% and contrast of 3.57). In both models the small chemical ligands were omitted during the initial refinement. Firstly, a ten-step rigid-body refinement using *REFMAC*5 (Murshudov *et al.*, 1997) was performed. The resulting *R* factors ($R_{\rm free}$) reached 33.7% (33.7%) and 43.2% (41.1%) for the models derived from the templates PDB entry 3e94 and PDB entry 1fby, respectively. An additional ten-step restrained refinement using *REFMAC*5 diminished the *R* factors ($R_{\rm free}$) to 28.5% (33.6%) and 31.6% (37.2%), respectively. In both cases, clear density was visible in the $F_{\rm o} - F_{\rm c}$ map and was attributed to the Sn atom of the ligand (Figs. 4*b* and 4*c*). In addition, the mobile aliphatic chains were also clearly visible in the $2F_{\rm o} - F_{\rm c}$ map (Fig. 4*c*).

As in the previously published structure of RXR–TBT (le Maire *et al.*, 2009), one TBT molecule is bound to two alternative conformations of Cys432 (Fig. 4*c*). Further refinements using *REFMAC*5 led smoothly to a very good model of the complex (Table 1).

In addition, *PHENIX* (Adams *et al.*, 2010) was also used for a fully automatic refinement. This procedure also led to the structure of the complex in a straightforward manner starting from the same templates (data not shown).

Finally, the structures of the RXR–TBT–Tif2 complex determined from data collected at room temperature and at 100 K were almost identical (Fig. 4*a*).

### 3.4. Crystal structure of unliganded CypD at room temperature

A new plate was used for setting up crystallization of CypD. The small number of crystals prevented the testing of ligand soaking in this case and the crystals were simply tested for diffraction quality and stability at room temperature under X-ray irradiation.

A 70% complete data set was readily obtained for CypD using only one crystal owing to its crystallization in a high-symmetry space group. A second crystal was used to collect a dozen additional images in order to increase the completeness to 86.2% with a multiplicity of 3.6 at a resolution of 1.54 Å (Table 1). These crystals were isomorphous to the cryocooled crystals (Colliandre & Guichou, unpublished work). Again, parallel molecular replacement was performed (see results at http://atome.cbs.cnrs.fr/AT2/EG/28727/atome.html). This structure at room temperature was solved starting from the structure of CypD obtained from a cryocooled crystal (PDB entry 2z6w; Kajitani *et al.*, 2008). After ten steps of rigid-body refinement and ten further steps of restrained refinement in *REFMAC*5 (Murshudov *et al.*, 1997), a good electron density appeared. It corresponded to the apo protein and included all residues from 44 to 207. Compared with the starting conformation, several side chains appeared to be reoriented and most of them were readily placed into the electron density using the 'Auto_Fit_rotamer' option in *Coot* (Emsley & Cowtan, 2004). The major rearrangement involves only one residue: Gly117. It is in two alternative conformations in the template, one of which was selected in the molecular-replacement step, while the other would have been closer to the actual structure at room temperature. To better match the electron density, the backbone of Gly117 was translated using the 'Rotate/Translate zone' option and a new round of restrained refinement was performed. It showed that Gly117 forms a hydrogen bond through its N atom to the side

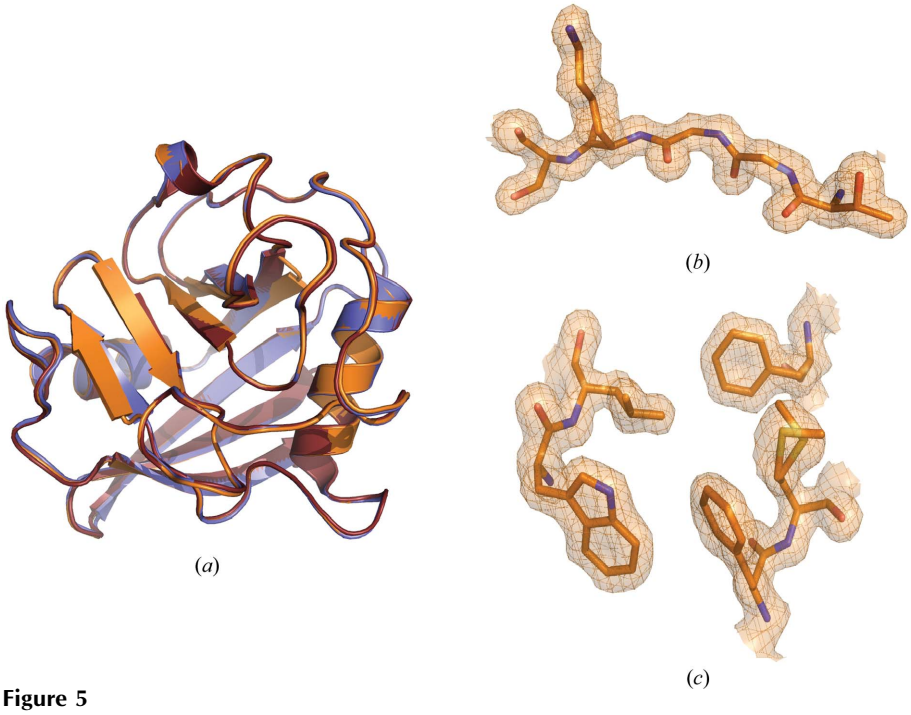


**Figure 5**
Crystal structures of cyclophilin CypD. (*a*) Superposition of the structure at room temperature of the unbound protein (PDB entry 3qyu; orange ribbon) with the equivalent structure at 120 K (PDB entry 2bit; magenta ribbon) and the structure bound to cyclosporin A (PDB entry 2r6w; blue ribbon). (*b*) Views of the $2F_{\rm o} - F_{\rm c}$ electron-density map in the region of Gly117 (residues 115–119). The map is contoured at 0.9$\sigma$. (*c*) Views of the $2F_{\rm o} - F_{\rm c}$ electron-density map in the active site for a set of hydrophobic residues lying in the active site (Met102, Phe103, Phe155, Trp163 and Leu164). The map is contoured at 0.9$\sigma$. This figure was generated using the program *PyMOL* (http://www.pymol.org).

chain of Thr110 (N—$O^{\gamma1}$ distance of ∼2.85 Å). A concomitant repositioning of the side chain of Arg124 allows another hydrogen bond to the carbonyl of Gly117 (O—$N^{\eta1}$ distance of ∼2.98 Å).

In addition, as a final round of rebuilding, several alternating side chains were built and some water molecules were added using *Coot*. This quick and semi-automatic rebuilding followed by restrained refinement using anisotropic *B* factors led to an optimal model with very good parameters (*R* factor and $R_{\rm free}$ of 15.1% and 19.3%, respectively; Table 1). Only minor changes were observed (Fig. 5*a*) between the template and the final structure solved at room temperature (r.m.s.d. of 0.29 Å over 164 $C^{\alpha}$ atoms). The latter slightly converged to the structure of the unbound CypD previously solved at 120 K (PDB entry 2bit; Schlatter *et al.*, 2005), showing an r.m.s.d. of 0.18 Å. All this may be a consequence of the fact that the template used for molecular replacement corresponds to the enzyme bound to its nanomolar inhibitor cyclosporin A (Kajitani *et al.*, 2008). This example shows that *in situ* measurement can yield excellent data at high resolution (see details of the electron density in Figs. 5*b* and 5*c*). Attempts to reproduce these crystals and soak them with ligands of interest will be made in the near future.

## 4. Discussion

In this study, we have successfully evaluated the use of new plates for crystal growth, for ligand soaking and finally for direct X-ray measurements without removing the crystals from the plate. This method takes advantage of the enhanced capabilities of the G-Rob robot for plate handling during data collection.

In the case of the protein kinase Erk-2, which crystallizes in a monoclinic space group, soaking and ligand detection were successfully performed for two distinct chemical compounds. Firstly, a data set was obtained at 83% completeness using three distinct crystals soaked with a purine derivative. Further optimization in the angle range accessible to the plate in the X-ray beam (from −25° to + 25° to −40° to + 40°) led to a 71% complete data set for the same protein using only one crystal. In both cases the ligands were clearly visible in the OMIT map.

For the nuclear receptor studied, which crystallizes in a high-symmetry space group, a complete data set was collected at 2.17 Å resolution. The deduced structure at room temperature perfectly matches that previously computed using diffraction from an equivalent but cryocooled crystal (le Maire *et al.*, 2009). In addition, comparisons of the statistics suggest that the main limit arises from the accessible multiplicity.

Finally, a high-resolution data set (1.54 Å) was obtained for another protein, human mitochondrial cyclophilin CypD. Although it was performed in the absence of added ligand, the atomic resolution (1.54 Å) and the quality of the resulting electron density indicate that ligands would readily be recognized upon binding. Data recorded on the same synchrotron beamline using a crystal mounted in a cryoloop (in the presence of an inhibitor; Colliandre & Guichou, to be published elsewhere), diffracting to the same resolution limit, showed very similar statistics (including $R_{\rm merge}$, *R* factor *etc.*).

While our first interest was to check the capacity of the setup to provide information on the mode of binding of potential ligands, alternative applications can also be envisaged. First of all, soaking with heavy-atom derivatives is promising. Secondly, the impact of additives on the diffraction quality can be tested rapidly. This will require further evaluation as well as the setting up of highly reproducible conditions for crystal growth. This step will remain a challenge for the use of the technique described here, although recent developments such as microseeding beads represent a promising tool, as exemplified with the proteins Erk-2 and CypD.

This project was funded by the CEA, the CNRS and the INSERM. The authors acknowledge financial support from the CNRS, INSERM, Institut Pasteur, Région Languedoc-Roussillon ('Chercheur d'Avenir') and ANR (Blanc 06-1_137054 and Jeune Chercheur ANR-07-JCJC-0046-CSD3). MG was supported by a grant from Région Languedoc-Roussillon and ALM was supported by a grant from ANR (ANR-07-PCVI-0001-01). We would like to thank Dr M. Cobb for the gift of the Erk-2 plasmid and Dr D. Schlatter for the gift of the CypD plasmid. We would like to thank Dr W. Bourguet for helpful discussions. We wish to acknowledge the help from the staff of beamlines BM-30 and ID14-2 at the ESRF in Grenoble, France. As a conflict of interest, we have to mention that JLF is a cofounder of the NatX-ray company (http://www.natx-ray.com/) and a member of its scientific advisory board.

## References

Adams, P. D. *et al.* (2010). *Acta Cryst.* D**66**, 213–221.
Bingel-Erlenmeyer, R., Olieric, V., Grimshaw, J. P. A., Gabadinho, J., Wang, X., Ebner, S. G., Isenegger, A., Schneider, R., Schneider, J., Glettig, W., Pradervand, C., Panepucci, E. H., Tomizaki, T., Wang, M. & Schulze-Briese, C. (2011). *Cryst. Growth Des.* **11**, 916–923.
Chessari, G. & Woodhead, A. J. (2009). *Drug Discov. Today*, **14**, 668–675.
Cymborowski, M., Klimecka, M., Chruszcz, M., Zimmerman, M. D., Shumilin, I. A., Borek, D., Lazarski, K., Joachimiak, A., Otwinowski, Z., Anderson, W. & Minor, W. (2010). *J. Struct. Funct. Genomics*, **11**, 211–221.
Egea, P. F., Mitschler, A., Rochel, N., Ruff, M., Chambon, P. & Moras, D. (2000). *EMBO J.* **19**, 2592–2601.
Emsley, P. & Cowtan, K. (2004). *Acta Cryst.* D**60**, 2126–2132.
Jacquamet, L., Ohana, J., Joly, J., Borel, F., Pirocchi, M., Charrault, P., Bertoni, A., Israel-Gouy, P., Carpentier, P., Kozielski, F., Blot, D. & Ferrer, J.-L. (2004). *Structure*, **12**, 1219–1225.
Joachimiak, A. (2009). *Curr. Opin. Struct. Biol.* **19**, 573–584.
Kajitani, K., Fujihashi, M., Kobayashi, Y., Shimizu, S., Tsujimoto, Y. & Miki, K. (2008). *Proteins*, **70**, 1635–1639.
le Maire, A., Grimaldi, M., Roecklin, D., Dagnino, S., Vivat-Hannah, V., Balaguer, P. & Bourguet, W. (2009). *EMBO Rep.* **10**, 367–373.
Leslie, A. G. W. (2006). *Acta Cryst.* D**62**, 48–57.
Murray, C. W. & Blundell, T. L. (2010). *Curr. Opin. Struct. Biol.* **20**, 497–507.

Murshudov, G. N., Skubák, P., Lebedev, A. A., Pannu, N. S., Steiner, R. A., Nicholls, R. A., Winn, M. D., Long, F. & Vagin, A. A. (2011). *Acta Cryst.* D**67**, 355–367.
Pons, J.-L. & Labesse, G. (2009). *Nucleic Acids Res.* **37**, W485–W491.
Pratt, D. J., Bentley, J., Jewsbury, P., Boyle, F. T., Endicott, J. A. & Noble, M. E. (2006). *J. Med. Chem.* **49**, 5470–5477.
Robinson, M. J., Harkins, P. C., Zhang, J., Baer, R., Haycock, J. W., Cobb, M. H. & Goldsmith, E. J. (1996). *Biochemistry*, **35**, 5641–5646.
Rose, P. W., Beran, B., Bi, C., Bluhm, W. F., Dimitropoulos, D., Goodsell, D. S., Prlic, A., Quesada, M., Quinn, G. B., Westbrook, J. D., Young, J., Yukich, B., Zardecki, C., Berman, H. M. & Bourne, P. E. (2011). *Nucleic Acids Res.* **39**, D392–D401.
Schlatter, D., Thoma, R., Küng, E., Stihle, M., Müller, F., Borroni, E., Cesura, A. & Hennig, M. (2005). *Acta Cryst.* D**61**, 513–519.
Schulz, M. N. & Hubbard, R. E. (2009). *Curr. Opin. Pharmacol.* **9**, 615–621.
Terwilliger, T. C., Adams, P. D., Moriarty, N. W. & Cohn, J. D. (2007). *Acta Cryst.* D**63**, 101–107.
Vagin, A. & Teplyakov, A. (2010). *Acta Cryst.* D**66**, 22–25.
Wang, Z., Cabagarajah, B. J., Boehm, J. C., Kassisa, S., Cobb, M. H., Young, P. R., Abdel-Meguid, S., Adams, J. L. & Goldsmith, E. J. (1998). *Structure*, **6**, 1117–1128.
Winn, M. D. *et al.* (2011). *Acta Cryst.* D**67**, 235–242.
Winn, M. D., Isupov, M. N. & Murshudov, G. N. (2001). *Acta Cryst.* D**57**, 122–133.
Xu, H. E., Lambert, M. H., Montana, V. G., Plunket, K. D., Moore, L. B., Collins, J. L., Oplinger, J. A., Kliewer, S. A., Gampe, R. T. Jr, McKee, D. D., Moore, J. T. & Willson, T. M. (2001). *Proc. Natl Acad. Sci. USA*, **98**, 13919–13924.
Zhang, F., Strand, A., Robbins, D., Cobb, M. H. & Goldsmith, E. J. (1994). *Nature (London)*, **367**, 704–711.